Asia Oceania Journal of Nuclear Medicine & Biology
http://aojnmb.mums.ac.ir
AOJNMB

Usefulness of respiratory-gated PET acquisition during delayed ^{18}F-FDG PET/CT scanning for patients with liver metastases

Shota Watanabe[1*], Kohei Hanaoka[1], Hayato Kaida[1, 2], Tomoko Hyodo[1, 2], Minoru Yamada[1, 2], Masakatsu Tsurusaki[1, 2], Kazunari Ishii[1, 2]

[1]Division of Positron Emission Tomography, Institute of Advanced Clinical Medicine, Kindai University Hospital, Osaka, Japan
[2]Department of Radiology, Kindai University Faculty of Medicine, Osaka, Japan

ARTICLEINFO

Article type:
Technical Note

Article history:
Received: 12 Nov 2020
Revised: 8 Jan 2021
Accepted: 13 Jan 2021

Keywords:
FDG
Liver metastases
Respiratory-gated technique
Dual-time-point PET/CT
Tumor-to-liver uptake ratio

ABSTRACT

Objective(s): To assess respiratory-gated (RG) positron emission tomography (PET) acquisition for patients with liver metastases during delayed PET/computed tomography (CT) scanning with fluorine-18-fluorodeoxyglucose (^{18}F-FDG).

Methods: Nineteen patients with liver metastases who had undergone early whole-body ^{18}F-FDG PET/CT scans without the RG technique and delayed scans with the RG technique were retrospectively selected. The maximum standardized uptake value (SUV_{max}) of 41 liver lesions and the tumor-to-liver uptake ratios (TLRs) for these same lesions were compared among three data sets: early non-respiratory-gated (early non-RG) images, delayed non-respiratory-gated (delayed non-RG) images, and delayed respiratory-gated (delayed RG) images. In the delayed non-RG and delayed RG images, the improvements in the TLR, relative to the early non-RG images, were assessed according to lesion size.

Results: For liver lesions, the SUV_{max} of early non-RG, delayed non-RG, and delayed RG images were 6.58±2.34, 7.69±3.08, and 9.47±3.73, respectively. There were significant differences among the three images ($P<0.01$). The TLR of the delayed RG images was significantly higher than those of the early non-RG and delayed non-RG images ($P<0.01$). In the delayed RG images, the difference in the TLR improvement for lesions ≤10 mm in size was 15% higher than that for lesions >10 mm in size; in the delayed non-RG images, the difference in the TLR improvement for the same lesion categories was 6%.

Conclusion: Delayed RG imaging improves the TLR, compared with early non-RG and delayed non-RG imaging, especially for small lesions. RG PET acquisition may be a promising protocol for assessing liver metastases on delayed PET/CT scans.

Please cite this paper as:

Watanabe S, Hanaoka K, Kaida H, Hyodo T, Yamada M, Tsurusaki M, Ishii K. Usefulness of respiratory-gated PET acquisition during delayed ^{18}F-FDG PET/CT scanning for patients with liver metastases. Asia Ocean J Nucl Med Biol. 2021; 9(2): 140-147. doi: 10.22038/AOJNMB.2021.53427.1365

Introduction

Positron emission tomography/computed tomography (PET/CT) with fluorine-18-fluorodeoxyglucose (^{18}F-FDG) has been reported to be useful for the management of patients with liver metastases (1). In addition, previous studies have suggested that the contrast between liver tumors and normal liver tissue on delayed ^{18}F-FDG images was higher than that for routine early imaging using dual-time-point ^{18}F-FDG PET/CT scans (2–5). The contrast improvement was correlated with an increase in ^{18}F-FDG accumulation in malignant tumors and a decrease in normal liver tissue for several hours after intravenous administration. According to Dirisamer et al., the maximum standardized uptake value (SUV_{max}) increased for 71 out of 81 malignant liver lesions (85%), while the mean SUV (SUV_{mean}) of normal liver tissue slightly decreased on delayed scans, compared with early scans (3). Moreover, Hassler et al. reported that on delayed scans, the SUV_{max} of liver lesions increased from 7.1±5.0 to 9.8±6.9, while the SUV_{max} of normal liver tissue decreased from

* *Corresponding author:* Shota Watanabe. Division of Positron Emission Tomography, Institute of Advanced Clinical Medicine, Kindai University Hospital, 377-2 Ohno-Higashi, Osakasayama, Osaka 589-8511, Japan .Tel: +81-72-366-0221; Fax: +81-72-367-1685; Email: shouta-w@med.kindai.ac.jp

2.8±0.7 to 2.4±0.6, compared with early scans (4). However, the delayed scans required a longer emission scan time than the early scans to mitigate the high noise level arising from the radioactive decay of ^{18}F (5).

On the other hand, a respiratory-gated (RG) technique is now available for PET/CT scans to suppress the effect of respiratory motion. The diagnostic usefulness of RG PET/CT scans has been assessed for various target organs, such as the lung, myocardium, pancreas, and liver (4, 6–12). For pulmonary and liver lesions, RG scans have been suggested to improve the SUV_{max}, diagnostic accuracy, and confidence (4, 10–12). Nevertheless, the feasibility of the RG technique, especially for visualizing liver metastases on delayed scans, has rarely been investigated in previous studies. It should be revealed whether non-RG image or RG image should be used in the delayed acquisition for the patients with liver metastases. In the present study, we focused on the delayed PET acquisition and assessed the usefulness of delayed RG PET acquisition, compared with a non-RG acquisition protocol, in patients with liver metastases.

Methods

Patients

In the present study, we retrospectively selected 19 patients with liver metastases (13 men and 6 women; mean age ± standard deviation, 68.7±11.7 years) who underwent early non-gated whole body ^{18}F-FDG PET/CT scanning without the RG technique and delayed abdominal scanning with the RG technique between November 2019 and March 2020. All the patients were diagnosed as having liver metastases using contrast-enhanced CT and/or gadolinium-ethoxybenzyl-diethylenetriamine penta-acetic acid (Gd-EOB-DTPA)-enhanced MRI and a clinical follow-up. The sites of the primary tumors in the recruited patients were the colorectum (n=12), stomach (n=3), lung (n=1), pancreas (n=1), breast (n=1), and bile duct (n=1). Finally, 41 lesions were used in our analysis. The patients fasted for at least four hours before the intravenous administration of 3.0 MBq/kg of ^{18}F-FDG (80.7–307.5 MBq). The blood sugar level was checked before administration, and none of the patients had a glucose level greater than 115 mg/dL.

This study was approved by the institutional review board of our institution; the need for prior informed patient consent was waived. Patient records and information were anonymized and were unidentifiable prior to the analysis.

PET/CT acquisition and image reconstruction

All the PET/CT imaging procedures were performed using a PET/CT scanner (Discovery PET/CT 710; GE Healthcare Life Sciences, Amersham Place, Little Chalfont, Buckinghamshire, England). The scanning protocol used in the present study is shown in Figure 1. For early non-gated whole body scans, non-respiratory-gated (early non-RG) images were acquired for 2 minutes per bed position at 57.2±4.2 minutes (approximately 60 minutes) after the administration of ^{18}F-FDG using the 3D time-of-flight mode (3D TOF), and helical CT data acquired with free breathing were used for attenuation correction.

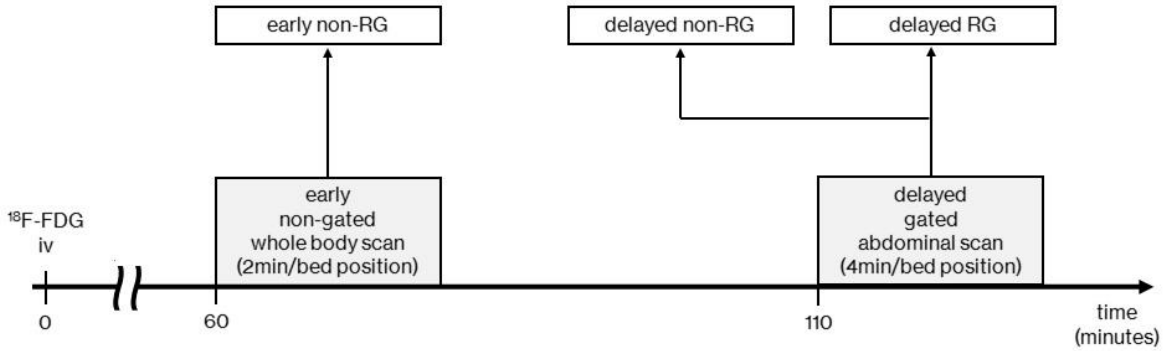

Figure 1. ^{18}F-FDG PET/CT protocol for patients with liver metastases in the present study

The CT scanning parameters were 120 kV, an automated tube current with a noise index of 23 for helical CT, 0.5 s/rotation, a pitch factor of 1.375, a detector configuration of 16×1.25 mm, a slice thickness of 3.75 mm, a slice interval of 3.27 mm, and a display field-of-view (DFOV) of 500 mm.

At 109.1±7.1 minutes (approximately 110 minutes) after the administration, delayed RG abdominal scanning was performed for 4 minutes per bed position using the list-mode acquisition. For respiratory motion tracking, a respiratory-gating system (Real-time Position

Management; Varian Medical Systems, Palo Alto, CA) was used. The respiratory waveforms were characterized using an infrared camera and reflective markers placed on the PET/CT scanner table and the patient's upper abdomen. The system measures the patient's respiratory pattern and range of motion and displays them as a waveform. For RG PET imaging, we used a gating method known as Q.static (GE Healthcare Life Sciences, Amersham Place, Little Chalfont, Buckinghamshire, England). This method is designed to extract a fraction of the PET data from the end-expiration quiescent portions of the patient breathing cycles (13). In delayed scan, we acquired for 4 minutes using list-mode. To investigate optimal delayed PET acquisition for liver metastases, we created the non-respiratory-gated (delayed non-RG) image and respiratory-gated (delayed RG) image from 4 minutes PET acquisition data and compared. The delayed RG image consisted of 2 minutes acquisition data since we used 50% PET data acquired after a 30% interval of one respiratory cycle from the detected inspiration point in the respiratory gating method used in this study. In addition, helical CT was performed to enable attenuation correction for the delayed non-RG and delayed RG images. The scanning parameters corresponded to those used for helical CT for early non-RG described in the previous paragraph.

All the PET images for early non-RG, delayed non-RG, and delayed RG scanning were reconstructed using a block sequential regularized expectation maximization algorithm (BSREM). The BSREM has a regularization parameter named the β value. The β value controls the strength of the regularizing term relative to the data statistics (14). In this study, we adopted a β value of 800. The PET imaging properties were as follows: slice thickness and interval of 3.27 mm, matrix size of 192×192, and DFOV of 500 mm.

PET image interpretation

For early non-RG, delayed non-RG, and delayed RG, voxels of interest (VOIs) were located at the same position in the liver lesion and the normal liver tissue. In the liver lesion, VOIs were set using a threshold technique to distinguish them from normal liver tissue, and the SUV_{max} was measured. The threshold value was 47.4±13.0%. The cubic VOIs were located in uniform normal liver as shown in Figure 2 and the size of VOIs were decided avoiding any liver lesions or the portal vein by referring to CECT and MRI images. The size of each cubic VOI used in normal liver tissue was 28×28×28 mm, and the SUV_{mean} was measured. The VOI size as a percentage of total liver volume was calculated from the formulae (liver volume (mL) = 706.2 × body surface area (m2) +2.4) reported by Urata et al. (15).

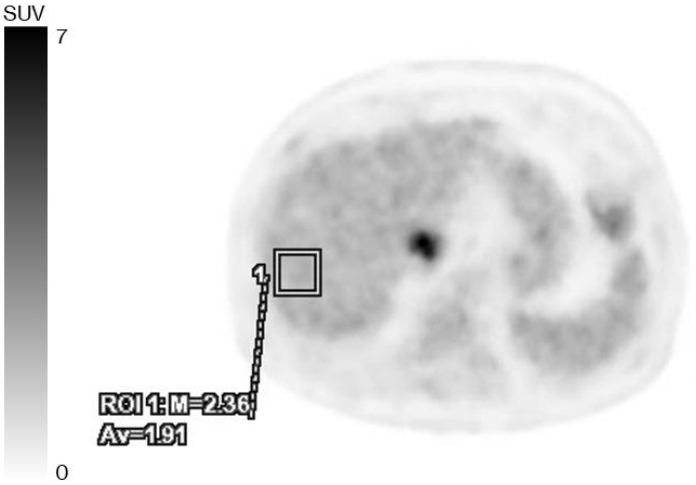

Figure 2. The cubic VOI locating in the normal liver tissue for measurement of SUV_{mean}

Moreover, the tumor-to-liver uptake ratio (TLR) was calculated by dividing the SUV_{max} for the liver lesion by the SUV_{mean} for normal liver tissue, since the TLR was previously reported to be the most useful parameter for detecting liver metastases (5). The TLR calculation was performed according to the previous reports by Dirisamer et al. and Lee et al. (3, 5). In addition, early whole body PET acquisition was generally performed under non-RG scanning because RG scanning required increasing scan time. Therefore, to compare the improvements in the TLRs of the delayed non-RG and delayed RG images, relative to the early non-RG images, the

improvement in the TLR was calculated using the following equation:

$$improvement\ in\ the\ TLR\ = \frac{TLR\ of\ delayed\ non\text{-}RG\ or\ TLR\ of\ delayed\ RG - TLR\ of\ early\ non\text{-}RG}{TLR\ of\ early\ non\text{-}RG} \times 100\ (\%)$$

The TLR improvements were compared according to the long axis of the lesion size: ≤10 mm or >10 mm as measured using CT and/or MRI images obtained with one month or less of the PET/CT and CT or MRI examinations. All the measurements were made using a computer workstation (Advantage Workstation 4.4; GE Healthcare Life Sciences, Amersham Place, Little Chalfont, Buckinghamshire, England).

Statistical analysis

For more accurate comparisons among the early non-RG, delayed non-RG, and delayed RG images, a statistical analysis was performed using SPSS Statistics 17.0 (SPSS; IBM, Tokyo, Japan). The SUV_{max}, SUV_{mean}, and TLR were analyzed using the Kruskal-Wallis one-way analysis of variance for ranks to compare overall differences among the three sets, and a post-hoc analysis was performed using the Wilcoxon signed-rank test with Bonferroni correction (n=3). A P value lower than 0.017 was considered statistically significant to account for the multiple sampling. The improvement in the TLR was compared according to lesion size between the delayed non-RG and the delayed RG using a Wilcoxon signed-rank test. Statistical signify-cance was defined as P <0.05.

Results

Quantitative analysis

The size of cubic VOIs measured in the normal liver tissue as a percentage of total liver volume was 1.9±0.2%. The resultant SUV_{max}, SUV_{mean}, and TLR values are summarized in Table 1. For the liver lesions, the SUV_{max} on the early non-RG, delayed non-RG and delayed RG images were 6.58±2.34, 7.69±3.08, and 9.47±3.73, respectively. The differences among the three image types were significant. For normal liver tissue, the SUV_{mean} for the delayed non-RG and delayed RG images were slightly lower than that for the early non-RG images. Consequently, the TLR of the early non-RG, delayed non-RG and delayed RG images were 2.68±1.03, 3.72±1.59, and 4.61±1.86, respectively.

Table 1. Resultant SUV_{max} in liver lesion, SUV_{mean} in normal liver tissue, and TLR for early non-RG, delayed non-RG and delayed RG images

	early non-RG	delayed non-RG	P value early non-RG) vs. delayed (non-RG	delayed RG	P value (early non-RG vs. delayed RG)	P value (delayed non-RG vs. delayed RG)
SUV_{max} in liver lesion	6.58±2.34	7.69±3.08	<0.01	9.47±3.73	<0.01	<0.01
SUV_{mean} in normal liver tissue	2.49±0.29	2.10±0.24	<0.01	2.08±0.24	<0.01	<0.01
TLR	2.68±1.03	3.72±1.59	<0.01	4.61±1.86	<0.01	<0.01

Note: early non-RG, early non-respiratory gated images; delayed non-RG, delayed non-respiratory gated images; delayed RG, delayed respiratory gated images; SUV_{max}, maximum standardized uptake value; SUV_{mean}, mean standardized uptake value; TLR, tumor-to-liver uptake ratio.

The differences among the three image types were significant, similar to the results for SUV_{max}. As shown in Table 2, despite categorization according to lesion size, the delayed RG images showed a significantly higher improvement in the TLR than the delayed non-RG images (P<0.01). For the delayed RG images, the improvement in the TLR of lesions ≤10 mm in size (n=17) was 15% higher than that for lesions >10 mm in size (n=24); for the delayed non-RG images, the difference in the improvement in TLR according to lesion size was 6%. Our data suggested that RG acquisition was effective for improving the TLR, especially for smaller lesions, as shown in Figure 3.

Table 2. Improvement in the TLR on delayed non-RG and delayed RG images

		delayed non-RG	delayed RG	P value
Improvement in the TLR	All lesions (n=41)	39±28%	75±44%	<0.01
	≤10 mm (n=17)	42±35%	83±57%	<0.01
	>10 mm (n=24)	36±22%	68±30%	<0.01

Note: delayed non-RG, delayed non-respiratory gated images; delayed RG, delayed respiratory gated images; TLR, tumor-to-liver uptake ratio.

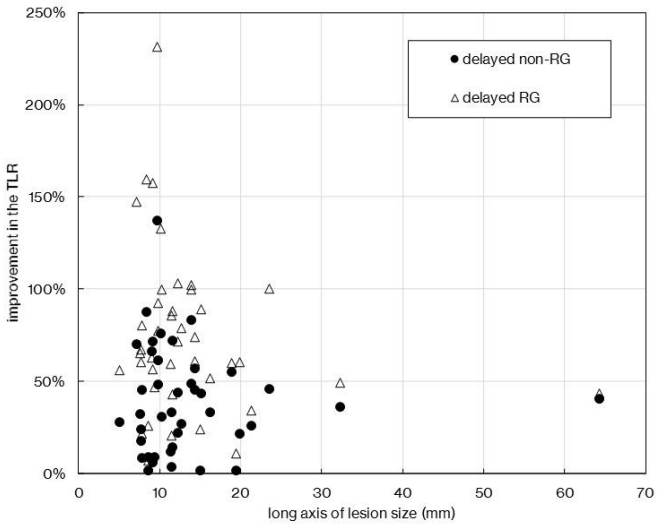

Figure 3. Scatter plot comparing the improvement in the TLR according to the long axis of the lesion for delayed non-RG and delayed RG images. The delayed RG images had a larger improvement in the TLR than the delayed non-RG images. This trend was especially true for lesions ≤10 mm in size

Clinical images

Figure 4 shows the PET and CT axial images for liver metastases detected in segment 6 (Couinaud classification). The TLRs of the early non-RG, delayed non-RG, and delayed RG images were 1.40, 1.52, and 2.05, respectively. Obviously, delayed RG scanning improved lesion conspicuity. The lesion size measured on the CECT image was 9.4×7.7 mm.

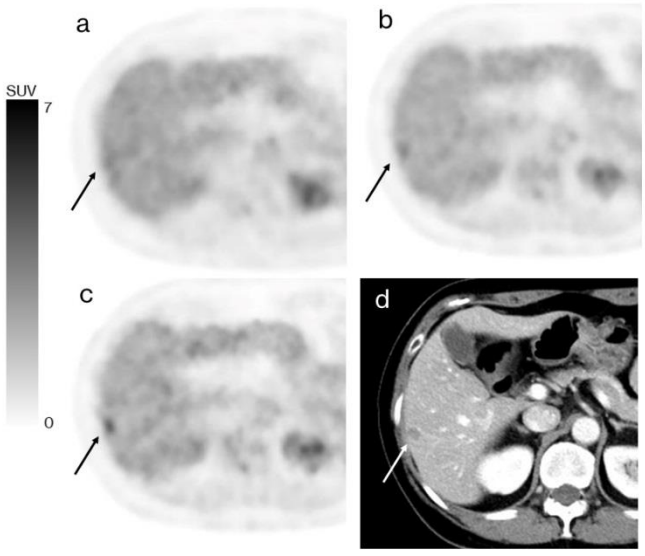

Figure 4. PET axial images obtained using (a) early non-RG, (b) delayed non-RG, and (c) delayed RG and (d) a contrast-enhanced CT axial image for a 64-year-old woman with liver metastasis. Both the delayed non-RG and the delayed RG images showed a lesion with a higher visibility than the early non-RG image. In addition, the delayed RG image showed the lesion more clearly than the delayed non-RG image because of the absence of the effect of respiratory motion

PET maximum intensity projection (MIP) images for liver metastases in segments 6, 7, and 8 obtained using early non-RG, delayed non-RG, and delayed RG scanning are shown in Figure 5.

The sizes of the small lesion marked by the thin arrow in Figure 5 (segment 7) and the other lesion marked by the bold arrow in Figure 5 (segment 8) were 5.2×5.0 mm and 11.5×8.8 mm,

respectively. The improvements in the TLR obtained using delayed non-RG and delayed RG scanning were 28% and 56% for the small lesion (segment 7) and 4% and 20% for the other lesion (segment 8), respectively. The improvement enabled by RG acquisition was more apparent for the small lesion.

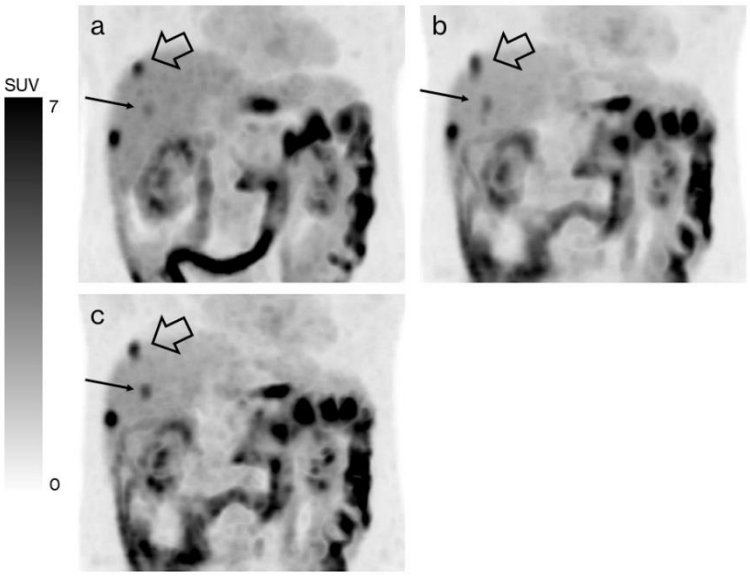

Figure 5. MIP PET images obtained using (a) early non-RG, (b) delayed non-RG, and (c) delayed RG in a 67-year-old man with liver metastases. The delayed RG image shows a small lesion more clearly (thin arrow) than the delayed non-RG image

Discussion

In the present study, we assessed RG PET acquisition during delayed ^{18}F-FDG PET/CT scanning using quantitative values such as the SUV_{max} in liver lesions, the SUV_{mean} in normal liver tissue, and the TLR. As a result, delayed RG scanning yielded a higher SUV_{max} and TLR than early non-RG and delayed non-RG scanning. Moreover, during delayed RG scanning, the improvement in the TLR for lesions ≤10 mm in size was 15% higher than that for lesions >10 mm in size. Thus, delayed RG was effective for improving the TLR of small lesions. To our knowledge, this finding has not been previously reported. Our data is of importance to ^{18}F-FDG PET/CT scanning because ^{18}F-FDG PET/CT reportedly has a relatively low sensitivity for the detection of liver metastases smaller than 10 mm (16).

Donati et al. compared the accuracy of lesion detection and the diagnostic confidence for liver metastases between ^{18}F-FDG PET/CT and Gd-EOB-DTPA-enhanced MRI, and they reported that the detection rates using ^{18}F-FDG PET/CT for lesions ≤10 mm in diameter and those >10 mm were 29% and 77%, respectively, while the detection rates using Gd-EOB-DTPA-enhanced MRI for lesions ≤10 mm in diameter and >10 mm were 71% and 90%, respectively (16). Therefore, small liver lesions can be difficult to detect using ^{18}F-FDG PET/CT. Tahari et al. compared the SUV_{max} according to lean body mass (SUL_{max}) in 40 pulmonary lesions (mean size ± standard deviation, 9.2±3.4 mm) and 24 liver lesions (10.2±2.8 mm) using initial conventional whole body scans without the RG technique and delayed scans with or without the RG technique. They reported that the benefit of the RG technique was small because the technique required a respiratory signal tracking device, additional software, and technical expertise to be performed correctly, although the mean percentage increase in the SUL_{max} for delayed images using the RG technique was 60.7±43.1%, compared with the results of an initial conventional whole body scan without the RG technique, in a series of 24 liver lesions. On the other hand, the improvement in the TLR for delayed RG scanning was significantly higher than that for delayed non-RG scanning in our study. In particular, this trend was more remarkable for smaller lesions with a size of ≤10 mm, suggesting that delayed RG could be helpful for detecting small lesions. Therefore, in delayed scans for small liver metastases, the RG technique should be initially used. The inclusion of RG acquisition in delayed ^{18}F-FDG PET/CT scanning protocols might help to overcome the limitations of ^{18}F-FDG PET/CT scanning, which has difficulty detecting small liver metastases. Accurate representations of ^{18}F-FDG uptake in

liver metastases can influence patient management, since ^{18}F-FDG uptake in liver metastases predicts the tumor response and recurrence after hepatectomy and ablation (17, 18).

Our result showed that SUV_{mean} in normal liver tissue for delayed non-RG image was significantly and slightly higher than that for delayed RG image. This trend might relate to the VOIs setting, the acquisition time for creating delayed non-RG image and delayed RG image. We located the cubic VOIs in the uniform accumulation region of normal liver tissue. Thus, the effect of respiratory motion was predicted to be slight. Moreover, we used the same list-mode 4 minutes acquisition data. Therefore, the delayed non-RG image and delayed RG image consisted of 4 minutes and 2 minutes data, respectively. Consequently, decreasing acquisition time used for creating images in the situation of negligibly slight effect of the respiratory motion might cause decrease SUV_{mean} in the uniform normal liver tissue.

In terms of delayed PET/CT scanning, our RG technique improved the SUV_{max} in liver lesions and the TLR without increasing the PET acquisition time or the radiation dose. On the other hand, Suenaga et al. performed RG PET/CT and non-RG PET/CT about 80 minutes after ^{18}F-FDG administration, and they reported no significant difference in the SUV_{max} for liver tumors between the RG PET images and the non-RG PET images (10). This difference might be related to not only the time interval between administration and PET acquisition, but also the reconstruction method that was used for the PET images. We used BSREM as the PET image reconstruction method, whereas Suenaga et al. performed ordered subset expectation maximization (OSEM). According to a previous investigation by Parvizi et al., which compared the properties of 41 liver metastases reconstructed using both BSREM and OSEM, BSREM yielded higher SUV_{max} values for liver lesions without an increase in image noise (19). Moreover, BSREM had better quantitative accuracy than OSEM (20). In the present study, the improvement in SUV_{max} enabled a higher TLR on the delayed RG images, compared with the delayed non-RG images. Thus, our results indicated that the synergistic effect of the RG technique and BSREM enabled an improvement in the TLR. Since TLR has been reported to be the most useful parameter for detecting hepatic metastases (5), the combined use of RG acquisition and BSREM might be suitable for delayed FDG/PET scanning in patients with liver metastases.

This study had certain limitations. First, there was a selection bias. The patients enrolled in the present study were selected after they had been diagnosed as having liver metastases. In addition, the final diagnosis of liver metastases was performed based on radiological findings and a clinical follow-up in all the patients, although the ideal gold standard for liver metastases would be histological confirmation. Second, we used helical CT acquired with free breathing for the attenuation correction. The mismatch between the CT and PET images as a result of respiratory motion can cause the mislocalization of small lesions and an insufficient quantitative accuracy based on attenuation correction error. However, 4DCT, which requires a larger radiation dose than helical CT, is necessary for RG CT. Therefore, 4DCT should be used in consideration of its necessity. Third, our patient population was relatively small, and we did not assess the diagnostic accuracy of our protocol for the detection of liver metastases. Hence, the present study was a preliminary study assessing the effect of the RG technique on delayed ^{18}F-FDG PET/CT scanning using quantitative values, and a clinical evaluation was not performed. In the future, we should assess the clinical usefulness of RG PET acquisition in delayed ^{18}F-FDG PET/CT imaging based on a large-scale case investigation. Fourth, we created non-RG image and RG image from the same list-mode acquisition data and compared the improvement in the TLR (%) based on early TLR with non-RG because early whole body PET acquisition was generally performed under non-RG scanning considering RG scanning required increasing scan time. However, if we calculated using early TLR with RG image, the improvement in the TLR (%) may be not significantly difference compared with non-RG image. Therefore, we should assess the improvement of TLR based on early TLR with RG in future work.

Conclusions

RG PET acquisition during delayed ^{18}F-FDG PET/CT scanning improved the TLR for liver metastases, especially small lesions. RG PET acquisition may be a promising protocol for assessing liver metastases on delayed PET/CT scans.

Acknowledgement

The authors would like to thank the staff of the Radiology Center, Kindai University Hospital for their assistance.

Funding

This research did not receive any specific grant from funding agencies in the public, commercial, or not-for-profit sectors.

Conflict of interest

No potential conflicts of interest were disclosed.

References

1. Sacks A, Peller PJ, Surasi DS, Chatburn L, Mercier G, Subramaniam RM. Value of PET/CT in the management of liver metastases, part 1. Am J Roentgenol. 2011; 197(2):W256–9 .
2. Koyama K, Okamura T, Kawabe J, Ozawa N, Higashiyama S, Ochi H, et al. The usefulness of ^{18}F-FDG PET images obtained 2 hours after intravenous injection in liver tumor. Ann Nucl Med. 2002; 16(3):169–76 .
3. Dirisamer A, Halpern BS, Schima W, Heinisch M, Wolf F, Beheshti M, et al. Dual-time-point FDG-PET/CT for the detection of hepatic metastases. Mol Imaging Biol. 2008; 10(6): 335–40 .
4. Hassler S, Hubele F, Constantinesco A, Goetz C. Comparing respiratory gated with delayed scans in the detection of colorectal carcinoma hepatic and pulmonary metastases with ^{18}F-FDG PET-CT. Clin Nucl Med. 2014;39(1):7–13 .
5. Lee JW, Kim SK, Lee SM, Moon SH, Kim TS. Detection of hepatic metastases using dual-time-point FDG PET/CT scans in patients with colorectal cancer. Mol Imaging Biol. 2011; 13(3):565–72 .
6. Frood R, McDermott G, Scarsbrook A. Respiratory-gated PET/CT for pulmonary lesion characterisation-promises and problems. Br J Radiol. 2018; 91(1086): 20170640 .
7. Bailly P, Bouzerar R, Shields T, Meyer ME, Daouk J. Benefits of respiratory-gated ^{18}F-FDG PET acquisition in lung disease. Nucl Med Commun. 2018; 39(1):44–50 .
8. Watanabe S, Hanaoka K, Shibata Y, Kaida H, Ishii K. Usefulness of respiratory-gated ^{18}F-FDG PET/CT scan protocol in patients having positive myocardial ^{18}F-FDG uptake. Nucl Med Commun. 2019; 40(3):235–41 .
9. Kasuya T, Tateishi U, Suzuki K, Daisaki H, Nishiyama Y, Hata M, et al. Role of respiratory-gated PET/CT for pancreatic tumors: A preliminary result. Eur J Radiol. 2013; 82(1):69–74 .
10. Suenaga Y, Kitajima K, Aoki H, Okunaga T, Kono A, Matsumoto I, et al. Respiratory-gated ^{18}F-FDG PET/CT for the diagnosis of liver metastasis. Eur J Radiol. 2013; 82(10):1696–701.
11. Crivellaro C, De Ponti E, Elisei F, Morzenti S, Picchio M, Bettinardi V, et al. Added diagnostic value of respiratory-gated 4D ^{18}F–FDG PET/CT in the detection of liver lesions: a multicenter study. Eur J Nucl Med Mol Imaging. 2018; 45(1):102–9 .
12. Tahari AK, Lodge MA, Wahl RL. Respiratory-Gated PET/CT versus Delayed Images for the Quantitative Evaluation of Lower Pulmonary and Hepatic Lesions. J Med Imaging Radiat Oncol. 2014; 58(3):277–82 .
13. Vallot D, Caselles O, Chaltiel L, Fernandez A, Gabiache E, Dierickx L, et al. A clinical evaluation of the impact of the Bayesian penalized likelihood reconstruction algorithm on PET FDG metrics. Nucl Med Commun. 2017; 38(11):979–84 .
14. Sah B-R, Stolzmann P, Delso G, Wollenweber SD, Hüllner M, Hakami YA, et al. Clinical evaluation of a block sequential regularized expectation maximization reconstruction algorithm in ^{18}F-FDG PET/CT studies. Nucl Med Commun. 2017; 38(1):57–66 .
15. Urata K, Kawasaki S, Matsunami H, Hashikura Y, Ikegami T, Ishizone S, et al. Calculation of child and adult standard liver volume for liver transplantation. Hepatology. 1995; 21(5):1317–21 .
16. Donati OF, Hany TF, Reiner CS, von Schulthess GK, Marincek B, Seifert B, et al. Value of retrospective fusion of PET and MR images in detection of hepatic metastases: comparison with ^{18}F-FDG PET/CT and Gd-EOB-DTPA-enhanced MRI. J Nucl Med. 2010; 51(5):692–9 .
17. Cornelis F, Storchios V, Violari E, Sofocleous CT, Schoder H, Durack JC, et al. ^{18}F-FDG PET/CT Is an Immediate Imaging Biomarker of Treatment Success After Liver Metastasis Ablation. J Nucl Med. 2016; 57(7):1052–7 .
18. Shim JR, Lee SD, Han SS, Lee SJ, Lee DE, Kim SK, et al. Prognostic significance of ^{18}F-FDG PET/CT in patients with colorectal cancer liver metastases after hepatectomy. Eur J Surg Oncol. 2018; 44(5):670–6 .
19. Parvizi N, Franklin JM, McGowan DR, Teoh EJ, Bradley KM, Gleeson F V. Does a novel penalized likelihood reconstruction of ^{18}F-FDG PET-CT improve signal-to-background in colorectal liver metastases? Eur J Radiol. 2015; 84(10):1873–8 .
20. Ahn S, Ross SG, Asma E, Miao J, Jin X, Cheng L, et al. Quantitative comparison of OSEM and penalized likelihood image reconstruction using relative difference penalties for clinical PET. Phys Med Biol. 2015; 60(15):5733–51 .